

Non-Gaussian Photon Correlations in Weakly Coupled Atomic Ensembles

YangMing Wang^{1,2,*} and Sahand Mahmoodian^{1,3,†}

¹*ARC Centre of Excellence for Engineered Quantum Systems,
School of Physics, The University of Sydney, Sydney, NSW 2006, Australia*

²*Sydney Quantum Academy, Sydney, NSW, Australia*

³*Institute for Photonics and Optical Sciences (IPOS),
School of Physics, The University of Sydney, NSW 2006, Australia*

(Dated: March 4, 2026)

We develop a scattering theory formalism and use it to predict that a resonantly driven atomic ensemble weakly coupled to an optical mode can generate light with non-Gaussian correlations. Our approach—based on a perturbative diagrammatic expansion of multi-photon interactions—shows that photon-photon interaction mediated by the emitters causes the transmitted light to have a connected third-order correlation function $g_c^{(3)}$ revealing its non-Gaussianity. We explain the temporal pattern of $g_c^{(3)}$ using the interaction processes in our diagrammatic expansion. A quantitative comparison with cascaded master equation simulations for small ensembles with optical depth $OD \leq 2$ confirms that the perturbative results remain accurate across experimentally relevant optical depths and for drive strengths large enough to make the predicted non-Gaussian signatures detectable. We anticipate that state-of-the-art nanofibre-coupled atomic ensembles can experimentally demonstrate our predictions.

Introduction.—Photon-photon interactions in optically driven atomic ensembles can alter the quantum state of an incident laser field. Here, the interplay of nonlinear interactions, due to the two-level atoms in the ensemble, and the elastic scattering of laser light out of the ensemble allows manipulating the quantum nature of light [1, 2]. For example, photons can become strongly correlated, modifying both intensity correlations [3–5] and electric field fluctuations [6, 7]. Such works have largely focused on quantifying two-body photon correlations. On the other hand, three-photon correlations, including non-Gaussian intensity and field correlations, have been measured in other quantum optics systems [8–12], and very recently an experiment using an atomic ensemble claimed to observe non-Gaussian light via the violation of the Siegert relation [13]. Here, We use the term “non-Gaussian” in two distinct senses. By non-Gaussian *field* correlations we mean that the output state is non-Gaussian in phase space (equivalently, its Wigner function is not Gaussian), in which case higher-order field moments are not fixed by first and second moments. By non-Gaussian *intensity* correlations we mean that normally ordered intensity cumulants beyond second order are nonzero, e.g., $g_c^{(3)} \neq 0$. Importantly, a Gaussian *field* state can still display non-Gaussian *intensity* correlations (thermal light is a standard example).

Despite experimental advances, a tractable theoretical framework for describing three-photon dynamics or the presence of non-Gaussian correlations in large atomic ensembles remains elusive. Dilute ensembles are often modeled using the Maxwell-Bloch equations [14–17], which, under a mean-field approximation, provide a minimal semiclassical description incorporating unidirectional coupling to a one-dimensional continuum of photon modes. To capture quantum correlations beyond the

mean-field level, one can employ a complete cascaded master equation [18, 19]. However, for large ensembles, the exponential growth of the Hilbert space with system size renders the direct computation of higher-order correlation functions, such as $g^{(3)}$, challenging, even if employing cumulant expansion [20, 21] or matrix-product operator [22, 23] methods.

In this work, we propose an analytic and diagrammatic framework to calculate up to three-photon transport through the atomic ensemble. Using the Maxwell-Bloch approach, the ensemble can be considered to be an array of atoms unidirectionally coupled to an optical nanofibre as shown in Fig. 1. The coupling efficiency between each atom and waveguide is weak $\beta \ll 1$ while the number of atoms $M \gg 1$, leading to significant optical depth $OD = 4\beta M$. Our diagrammatic approach takes advantage of the weak coupling and uses β as an expansion parameter, enabling us to analytically compute leading-order contributions to the three-photon-correlated component of the wavefunction and the connected third-order correlation function $g_c^{(3)}$. So far, our perturbative approach is the only way to analytically compute three-photon interactions, which is the cause of non-Gaussian field correlation, in *large* atomic ensembles. To show that the outgoing state after transport has non-Gaussian field correlation, we demonstrate that $g_c^{(3)}$ calculated from our approach disagrees with $\tilde{g}_c^{(3)}$ calculated by Isserlis’s theorem based on the hypothesis that the state is a Gaussian field.

Model.—The model for our system is depicted in Fig. 1, where M atoms are unidirectionally coupled to a propagating channel in a waveguide. Here we have illustrated the example of a nanofibre geometry where atoms are trapped near the fibre and interact via its evanescent field. Each atom couples to the propagating channel at

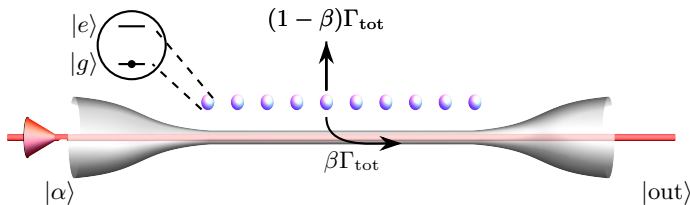


FIG. 1. An array of M chirally coupled two-level atoms (depicted as blue balls) resonantly driven by an external coherent field $|\alpha\rangle$ producing a strongly correlated output photon state $|\text{out}\rangle$. Each atom couples to the waveguide with a decay rate $\beta\Gamma_{\text{tot}}$ and to external loss channel with a decay rate $(1-\beta)\Gamma_{\text{tot}}$.

rate $\Gamma = \beta\Gamma_{\text{tot}}$ and to its individual loss channel at rate $\gamma = (1-\beta)\Gamma_{\text{tot}}$, where β quantifies the coupling efficiency and Γ_{tot} is the overall atomic decay rate. The emitters are driven by a resonant coherent driving field from one end of the waveguide. The emitter spacing exceeds one resonant wavelength of the two-level atoms which ensures negligible collective emission outside the waveguide. Typical experimental values for atomic ensembles coupled to nanofibres yield $\beta \sim 0.01$ [3]. Despite the small individual coupling strength, the OD of the entire atomic array becomes significant $\text{OD} = \mathcal{O}(1)$, where $\mathcal{O}(\cdot)$ indicates big-O notation. This enables the collective nonlinear effects and strong dissipation to substantially modulate photon transport properties, which, as we show, results in strongly correlated photons and non-Gaussian output states of light.

The local scattering event at the m th atom is described by a one-dimensional two-channel model, where each atom interacts with the waveguide and a loss channel. The Hamiltonian is (with $\hbar = c = 1$),

$$\hat{H}_m = \int_{-\infty}^{\infty} dx \left\{ \hat{a}^\dagger(x)(-i\partial_x)\hat{a}(x) + \hat{b}_m^\dagger(x)(-i\partial_x)\hat{b}_m(x) + \delta(x) \left[\hat{\sigma}_m^+ (\sqrt{\Gamma}\hat{a}(x) + \sqrt{\gamma}\hat{b}_m(x)) + \text{h.c.} \right] \right\}, \quad (1)$$

where $\hat{a}^\dagger(x)$ and $\hat{b}_m^\dagger(x)$ create photons in the propagating and m th atom's loss channels respectively, while $\hat{\sigma}_m^\pm$ are Pauli operators for the m th two-level emitter.

By applying the following Weyl transformation, $\hat{a}_m^{(e)}(x) = \sqrt{\beta}\hat{a}(x) + \sqrt{1-\beta}\hat{b}_m(x)$, $\hat{a}_m^{(o)}(x) = \sqrt{1-\beta}\hat{a}(x) - \sqrt{\beta}\hat{b}_m(x)$, (1) splits into two decoupled even and odd channels. The odd channel Hamiltonian $\hat{H}_m^{(o)}$ describes non-interacting transport. All the information about atom-photon and photon-photon interactions at the m th atom is encoded in the even

channel Hamiltonian $\hat{H}_m^{(e)}$ with interaction strength Γ_{tot} ,

$$\hat{H}_m = \hat{H}_m^{(e)} + \hat{H}_m^{(o)}, \quad \hat{H}_m^{(o)} = \int_{-\infty}^{\infty} dx \hat{a}_m^{\dagger(o)}(x)(-i\partial_x)\hat{a}_m^{(o)}(x)$$

$$\hat{H}_m^{(e)} = \int_{-\infty}^{\infty} dx \left\{ \hat{a}_m^{\dagger(e)}(x)(-i\partial_x)\hat{a}_m^{(e)}(x) + \delta(x)\sqrt{\Gamma_{\text{tot}}}\left[\hat{\sigma}_m^+\hat{a}_m^{(e)}(x) + \text{h.c.}\right] \right\}. \quad (2)$$

The n -photon scattering in the even subspace can be fully described by the S -matrix derived from Bethe's Ansatz [24, 25]. The full S -matrix element encodes all the information of free propagation of photons, photon-atom and photon-photon interactions. We refer to free propagation of photons and individual elastic photon-atom scattering as *disconnected processes* because they factorize into independent terms in the S -matrix. The *connected part* of S -matrix is defined by subtracting all the products of the disconnected processes from the full S -matrix, enabling us to extract the genuine effects of n -body photon-photon interactions [26]. The expression of the full and connected two- and three-photon S -matrix is given in the accompanying work [27].

The local scattering event at the m th atom can be calculated by the following steps: (1) transform the incoming state from the propagating channel into even/odd channel picture (2) multiply the term with n even photons by the n -photon S -matrix (3) transform back to propagating/loss channel picture. When the photon remains in the waveguide, elastic single-photon scattering reduces to multiplication by the k -space transmission coefficient $t_k = 1 - i\beta\Gamma_{\text{tot}}/(k + i\Gamma_{\text{tot}}/2)$, [1, 28] while two- and three-photon interaction events are captured by the multiplications of their respective connected scattering matrices $\beta^2\hat{S}_{p_1p_2,k_1k_2}^C$ and $\beta^3\hat{S}_{p_1p_2p_3,k_1k_2k_3}^C$. When a photon is lost by elastic scattering out of the waveguide, the incoming state is multiplied by a reflection coefficient $r_k = -\sqrt{\beta(1-\beta)}i\Gamma_{\text{tot}}/(k + i\Gamma_{\text{tot}}/2)$. Alternatively, if loss occurs immediately after a two- or three-photon interaction, the incoming state is multiplied by $\beta^{3/2}\sqrt{(1-\beta)}\hat{S}_{p_1p_2,k_1k_2}^C$ or $\beta^{5/2}\sqrt{(1-\beta)}\hat{S}_{p_1p_2p_3,k_1k_2k_3}^C$ respectively.

Expressing the scattering in terms of the connected part of the S -matrix clarifies the way in which genuine photon-photon interactions scale with the various powers of coupling strength β . Since $\beta \ll 1$, this scaling behavior motivates us to perturbatively treat the effect of photon-photon interactions in terms of the order in β . If a three-photon transport process has no photon-photon interaction, the outgoing state is simply the incoming state of the array multiplied by t_0^{3M} . Transport processes generating three-photon correlations are the main interest of this work. In Fig. 2, we sketch the interaction processes where three-photon trajectories are connected by interaction lines. These diagrams are drawn according

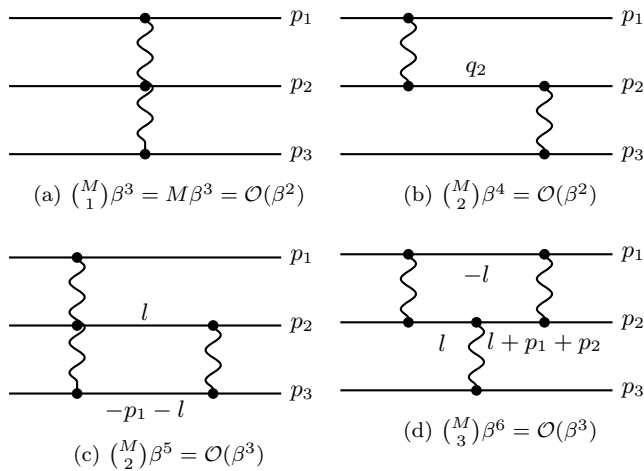


FIG. 2. Diagrammatic representation of the terms in $T^{(1)}$, which is the major contribution to the non-Gaussianity of outgoing light. The diagram including one three-photon interaction is called 3-vertex diagram, and the diagram including two two-photon interactions is called 4-vertex diagram. The momentum of the photons after the interaction is labeled above the horizontal line. The line piece without momentum labels mean the photon is on resonance with the atom. The order estimates below each diagram show their respective scaling behavior in the large optical depth regime.

to the following rules: (1) Each horizontal line indicates the trajectory of each photon being transported through the array from the left to the right. The individual elastic atom-photon scatterings are not explicitly indicated on the line. (2) Each black circular dot on the photon trajectory represents an atomic site where the photon interacts with other photons. The dots on the same column corresponds to the same atomic site. (3) A n -photon interaction is represented by a wavy line connecting n dots. We note that black dots can be any atom in the array, therefore each diagram in Fig. 2 represents all possible transport processes with the interactions happening on different atomic sites. For example, Fig. 2(a) shows three photons interacting via a single atom. This can occur at any atom within the ensemble and therefore the amplitude of this type of processes has a combinatorial factor of M . Photon-photon interactions at the start of the ensemble are more likely as on-resonant photon transports are lossy. Each elastic scattering before the photon-photon interaction multiplies the photon wavefunction by t_0 , exponentially decreasing its amplitude along the array.

Based on the transport processes sketched in Fig. 2, the scattering matrices for the 3- and 4-vertex diagrams can be written as follows. For resonant input photons, the 3-vertex diagram (Fig. 2(a)) is expressed as

$$\hat{T}^{3v} = \sum_{j=0}^{M-1} (t_{p_1} t_{p_2} t_{p_3})^{M-j-1} \beta^3 \hat{S}_{p_1 p_2 p_3, 000}^C t_0^{3j}, \quad (3)$$

where each term describes j individual single-photon scatterings, followed by a three-photon interaction at site $j+1$, and the remaining $M-j-1$ individual single-photon scatterings. For the 4-vertex diagram (Fig. 2(b)),

$$\hat{T}^{4v} = \sum_{j=0}^{M-2} \sum_{m=0}^{M-j-2} t_{p_1}^{M-j-1} (t_{p_2} t_{p_3})^{M-j-m-2} \beta^2 \hat{S}_{p_2 p_3, q_2 0}^C \times t_{q_2}^m \beta^2 \hat{S}_{p_1 q_2, 00}^C t_0^{3j+m+1}, \quad (4)$$

where after j individual single-photon scatterings, the first two-photon interaction occurs at site $j+1$; the middle photon with momentum q_2 then undergoes m additional individual single-photon scatterings before the second two-photon interaction at site $j+m+2$, followed by the remaining $M-j-m-2$ individual single-photon scatterings. Due to the bosonic symmetry, there are six 4-vertex diagrams corresponding to different permutations of the outgoing momenta p_1, p_2, p_3 at the right end of the diagram. To estimate the order of the amplitude of each diagram for perturbative expansion, we need to consider (i) the weight of the coupling constant β , and (ii) the combinatorics of the process due to interactions potentially occurring at any atom in the ensemble. For (i), we follow how photon-creation operators transform under Weyl transformation for nonlinear interactions. Each transmitted photon picks up a factor $\sqrt{\beta}$ when moving from the propagating to the even channel and another $\sqrt{\beta}$ when transforming back to the propagating channel, giving an overall factor β . This means the wavefunction amplitude of a single two-photon interaction scales as β^2 , while a single three-photon interaction scales as β^3 . For a lost photon, the second factor becomes $\sqrt{1-\beta}$, so the vertex contributes $\sqrt{\beta(1-\beta)} \approx \sqrt{\beta}$. For (ii), the combinatorics of a diagram with n photon-photon interactions is $\binom{M}{n}$. For larger OD $\beta M = \mathcal{O}(1)$, the order of magnitude of a diagram is estimated by multiplying β and the combinatorial factor. For example, the order of Fig. 2b is $\binom{M}{2} \beta^4 \approx M^2 \beta^4 = \mathcal{O}(\beta^2)$. For the order estimation in small or intermediate OD, because the power of β is fixed for each diagram, the amplitude of the diagram grows monotonically with M , therefore the leading diagrams at small or intermediate OD are a subset of those at large OD. Hence, perturbative results derived for the large-OD regime remain valid, and even gain higher accuracy, when applied to lower-OD systems.

From the Eq. 3 and 4, we see that at large OD, \hat{T}^{3v} and \hat{T}^{4v} are both at $\mathcal{O}(\beta^2)$, which is the leading-order contribution among all possible three-photon-connected diagrams. The subleading order $\mathcal{O}(\beta^3)$ three-photon connected diagrams includes two types of diagrams: (1) the diagrams with one three-photon interaction and one two-photon interaction, and (2) the diagrams with three two-photon interactions. One representative of each type is shown in Figs. 2c and 2d. The subleading order diagrams are negligible at $\beta \approx 1\%$, but make modest quan-

tuitive corrections on top of the leading order diagrams at large OD with $\beta \approx 5\%$. As the diagrams feature a loop structure, we refer to these as loop-order diagrams and their explicit calculation is presented in our accompanying work [27].

So far, we only considered the incoming state of the array as a three-photon Fock state. For an on-resonance coherent state input $|\alpha\rangle = e^{-|\alpha|^2/2} \sum_{n=0}^{\infty} \frac{P_{\text{in}}^{n/2}}{n!} \int_{-L/2}^{L/2} \prod_{j=1}^n dx_j \hat{a}^\dagger(x_j) |0\rangle$, where L is the quantization length, and $P_{\text{in}} = |\alpha|^2/L$ is the input power. In the thermodynamic limit $L, |\alpha|^2 \rightarrow \infty$ with fixed P_{in} . To apply our scattering theoretic approach for coherent input, we employ the following assumption: In the n -photon component of the coherent input, we assume that exactly k photons participate in the interaction processes represented by a given k -photon diagram (with $k = 3$ presented in Fig. 2), while the remaining $n - k$ photons scatter independently (being transmitted or lost one by one). Consequently, the amplitude for that n -photon sector factorizes into the product of k -photon diagram amplitude multiplied by the single-photon amplitudes for the other $n - k$ photons; the full output is obtained by summing this factorized contribution over n and every allowed configuration of the extra $n - k$ photons.

Connected third-order correlation function.—Having identified the leading-order contributions to connected three-photon scattering, we now translate this into an experimentally accessible quantity that reflects both non-Gaussian intensity and field correlation in the outgoing light. The connected third-order correlation function is defined as

$$g_c^{(3)}(x_1, x_2, x_3) = 2 + g^{(3)}(x_1, x_2, x_3) - \sum_{i < j} g^{(2)}(x_i, x_j), \quad (5)$$

where $g^{(2)}(x_1, x_2)$ and $g^{(3)}(x_1, x_2, x_3)$ are the normalized second- and third-order correlation functions, respectively. For non-vanishing power, $g_c^{(3)}(x_1, x_2, x_3)$ vanishes when either one photon is far away from the other two, or when the intensity correlation is Gaussian [8, 29, 30]. Moreover, if the state of light has only Gaussian field correlation, both $g^{(3)}$ and $g^{(2)}$ can be determined by the second-order moment and mean of $\hat{a}(x)$ and $\hat{a}^\dagger(x)$ by Isserlis's theorem [31–33]. In the weak driving condition $\mathcal{O}(P_{\text{in}}/\Gamma_{\text{tot}}) = \mathcal{O}(\beta)$ [34], $g^{(n)}(x_1, \dots, x_n) = \langle : \prod_{j=1}^n \hat{a}^\dagger(x_j) \hat{a}(x_j) : \rangle / \prod_{k=1}^n \langle \hat{a}^\dagger(x_k) \hat{a}(x_k) \rangle$ for $n = 2, 3$ can be approximated as:

$$\begin{aligned} g^{(3)}(x_1, x_2, x_3) &\approx |\psi_3(x_1, x_2, x_3)|^2 / t_0^{6M}, \\ g^{(2)}(x_1, x_2) &\approx |\psi_2(x_1, x_2)|^2 / t_0^{4M}, \end{aligned} \quad (6)$$

where $\psi_2(x_1, x_2) = t_0^{2M} + \phi_2(x_1, x_2)$ with $\phi_2(x_i, x_j)$ is the entangled wavefunction generated by all possible two-photon interactions. The output power $\langle \hat{a}^\dagger(x) \hat{a}(x) \rangle \approx P_{\text{in}} t_0^{2M}$, $\psi_3(x_1, x_2, x_3) = t_0^{3M} + t_0^M \sum_{1 \leq i < j \leq 3} \phi_2(x_i, x_j) +$

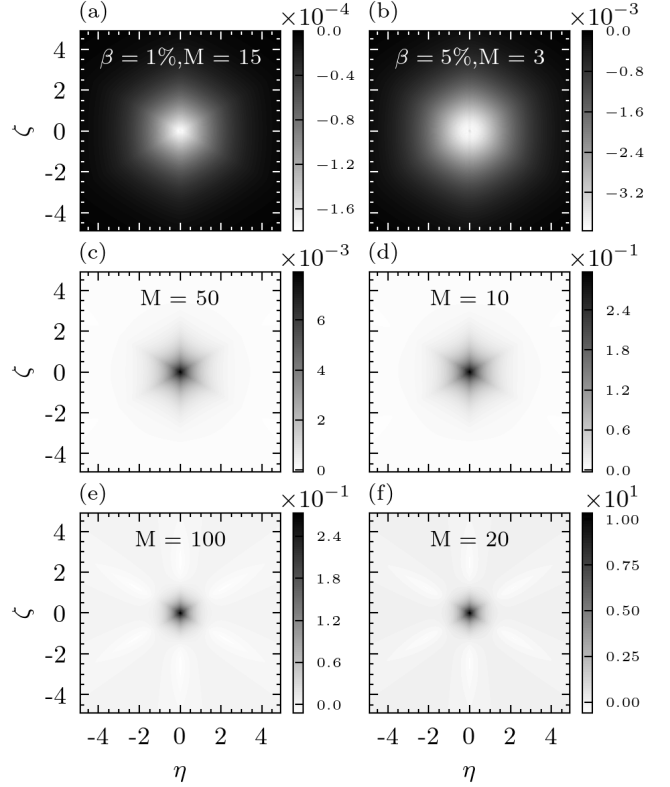


FIG. 3. Connected third-order correlation function with various OD $g_c^{(3)}(R, \eta, \zeta)$ in Jacobi coordinates, with center of mass $R = 0$. The six-fold symmetry reflects three symmetry axes corresponding to two-photon coincidences. $g_c^{(3)}$ is computed at tree-level diagram for $\beta = 1\%$ while the loop order correction is added for $\beta = 5\%$

$\phi_3(x_1, x_2, x_3)$, where ϕ_3 encodes the correlation induced by leading- and subleading-order three-photon interactions depicted in Fig. 2. We evaluate ϕ_2 and ϕ_3 analytically, but for brevity here, their expressions are given in [27].

In Fig. 3 we plot the connected third-order correlation $g_c^{(3)}(x_1, x_2, x_3)$ using the approximation (6) for an atomic ensemble with $\beta = 1\%$ and 5% . The value $\beta = 1\%$ represents the approximate value from past experiments [3, 6, 20], while $\beta = 5\%$ is what could be obtained if the atoms are trapped more closely to the fibre and/or if the light-matter coupling is enhanced, for example, with slow light using fibre gratings. The result of $g_c^{(3)}(x_1, x_2, x_3)$ is shown in Jacobi coordinates $R = \frac{x_1 + x_2 + x_3}{\sqrt{3}}$, $\eta = \frac{x_1 - x_2}{\sqrt{2}}$, $\zeta = \sqrt{\frac{2}{3}} \left(\frac{x_1 + x_2}{2} - x_3 \right)$ with $R = 0$ fixed by translational invariance. In the η - ζ plane, the value of $g_c^{(3)}$ at the origin $(\eta, \zeta) = (0, 0)$ corresponds to a three-photon coincidence $x_1 = x_2 = x_3$, i.e., enhanced (positive) or suppressed (negative) simultaneous detection of all three photons. Three axes $\eta = 0$, $\zeta = \sqrt{3}/3\eta$ and $\zeta = -\sqrt{3}/3\eta$ corresponding to two-photon coincidence events with the third photon sepa-

rated (except at their intersection $(0,0)$). $g_c^{(3)}$ is symmetric with respect of the three axes because of bosonic permutation symmetry. Furthermore, this three-fold symmetry is doubled to be a six-fold symmetry because $g_c^{(3)}$ does not distinguish whether a photon pair arrives before or after the lone photon.

As the optical depth increases, $g_c^{(3)}$ evolves from being everywhere negative, through a regime of uniform positivity, to a characteristic pattern with a bright central peak surrounded by six negative “outer legs.” Under approximation (6), $g_c^{(3)}(x_1, x_2, x_3) = 2\phi_3(x_1, x_2, x_3)/t_0^{3M} + 2[\sum_{(i,j,k) \in A} \phi_2(x_i, x_j)\phi_2(x_j, x_k)]/t_0^{4M} + \mathcal{O}(\beta^3)$, where $A = \{(1, 2, 3), (2, 1, 3), (1, 3, 2)\}$. In contrast, if we hypothesize that the outgoing state has only Gaussian field correlation, Isserlis’s theorem gives $\tilde{g}_c^{(3)}(x_1, x_2, x_3) = 2[\sum_{(i,j,k) \in A} \phi_2(x_i, x_j)\phi_2(x_j, x_k)]/t_0^{4M} + \mathcal{O}(\beta^3)$ [27, 31]. Hence, $g_c^{(3)}$ becomes the sum of two parts: (i) the amplitude of correlated three-photon wavefunction ϕ_3 (included in the first term and the high-order terms collected in $\mathcal{O}(\beta^3)$), (ii) the product amplitude of correlated two-photon wavefunctions $\phi_2\phi_2$. Non-Gaussian intensity correlation therefore have contributions from terms with (i) non-Gaussian and (ii) Gaussian field correlations.

In the following, we explain the spatial pattern in Fig. 3 in terms of the relative amplitude of various transport processes in Fig. 2 and two-photon interaction. From the formulae of Weyl transformation, we see that without photon loss, a n -photon interaction at an emitter multiplies a factor of β^n ($n=2,3$) on the corresponding wavefunction amplitude. At low OD $4\beta M = 0.6$, ϕ_3 is dominated by the scattering amplitude of the process, whose sign is also negative, depicted in Fig. 2a where three-photon interaction only happens once during transport, having a factor of β^3 and ϕ_2 is dominated by a single two-photon interaction transport having a factor of β^2 . The $\phi_2\phi_2$ part of $g_c^{(3)}$ is negligible at low OD plotted in Fig. 3(a),(b). As the optical depth increases, e.g., to $4\beta M = 2$, more atom sites are available to accommodate photon-photon interactions. Sequential photon-photon interactions in the transports results in the accumulation of the amplitude of processes with positive sign in both the ϕ_3 and $\phi_2\phi_2$. In ϕ_3 , the process involving two successive two-photon interactions (Fig. 2b) grows in importance because it is enhanced by the combinatorial factor $\binom{M}{2}$ counting the choice of two emitter sites. At the same time, the magnitude of ϕ_2 itself becomes larger since the leading single two-photon interaction contribution is enhanced by a combinatorial factor M from the M possible sites at which the two-photon interaction can occur. At large OD $4\beta M = 4$, $\phi_2\phi_2$ dominates as the ϕ_3 term is weighted by one more factor of t_0^M exponentially decaying with OD. Here, $g_c^{(3)}$ becomes approximately proportional to $\phi_2\phi_2$. Its spatial pattern in Fig. 3 (e),(f) can be explain solely from the position space behavior of ϕ_2 : ϕ_2

is negative when two photons are nearly coincident and positive when they are at moderate separation. Hence, the product $\phi_2(x_i, x_j)\phi_2(x_j, x_k)$ is positive when three photon coincide and is negative when one is far from the other two. To visualize the violation from Isserlis’s theorem, we calculate $g_c^{(3)} - \tilde{g}_c^{(3)}$ (in Fig. S3).

For a small number of atoms ($M \leq 11$), both $g_c^{(3)}$ and $\tilde{g}_c^{(3)}$ can be computed numerically using the quantum regression theorem (QRT) together with the cascaded master equation. As shown in Fig.S4, although $g_c^{(3)}$ and $\tilde{g}_c^{(3)}$ decrease at higher input power $P_{in} \geq 0.4\Gamma_{tot}$, the simulations remain in qualitative agreement with the theory for $OD > 1$. The signal strength of $g_c^{(3)}$ is discussed in Supplementary Material and our accompanying work [27].

Conclusion.—We have developed a diagrammatic scattering theory to calculate three-photon transport through weakly coupled atomic ensembles. Our formalism provides analytic expression of the leading-order processes that contribute to non-separable three-photon correlations. We have used our new approach to predict the presence of non-Gaussian intensity and field correlations in the transmitted field of coherently driven atomic ensembles. We anticipate our results will pave the way for experimental demonstration of sources of non-Gaussian photon states using atoms coupled to nanofibres.

Acknowledgements.—S.M. acknowledges support from the Australian Research Council (ARC) via the Future Fellowship, ‘Emergent many-body phenomena in engineered quantum optical systems’, project no. FT200100844. Y.W. acknowledges the financial support from Sydney Quantum Academy, Sydney, NSW, Australia.

* ywan8652@uni.sydney.edu.au

† sahand.mahmoodian@sydney.edu.au

- [1] S. Mahmoodian, M. Čepulkovskis, S. Das, P. Lodahl, K. Hammerer, and A. S. Sørensen, Strongly correlated photon transport in waveguide quantum electrodynamics with weakly coupled emitters, *Phys. Rev. Lett.* **121**, 143601 (2018).
- [2] A. S. Sheremet, M. I. Petrov, I. V. Iorsh, A. V. Poshakinskiy, and A. N. Poddubny, Waveguide quantum electrodynamics: Collective radiance and photon-photon correlations, *Rev. Mod. Phys.* **95**, 015002 (2023).
- [3] A. S. Prasad, J. Hinney, S. Mahmoodian, K. Hammerer, S. Rind, P. Schneeweiss, A. S. Sørensen, J. Volz, and A. Rauschenbeutel, Correlating photons using the collective nonlinear response of atoms weakly coupled to an optical mode, *Nat. Photonics* **14**, 719 (2020).
- [4] M. Cordier, M. Schemmer, P. Schneeweiss, J. Volz, and A. Rauschenbeutel, Tailoring photon statistics with an atom-based two-photon interferometer, *Phys. Rev. Lett.* **131**, 183601 (2023).
- [5] G. Ferioli, I. Ferrier-Barbut, and A. Browaeys, Emergence of second-order coherence in the superradiant emis-

- sion from a free-space atomic ensemble, Phys. Rev. Lett. **134**, 153602 (2025).
- [6] J. Hinney, A. S. Prasad, S. Mahmoodian, K. Hammerer, A. Rauschenbeutel, P. Schneeweiss, J. Volz, and M. Schemmer, Unraveling two-photon entanglement via the squeezing spectrum of light traveling through nanofiber-coupled atoms, Phys. Rev. Lett. **127**, 123602 (2021).
- [7] Z. H. Lu, S. Bali, and J. E. Thomas, Observation of squeezing in the phase-dependent fluorescence spectra of two-level atoms, Phys. Rev. Lett. **81**, 3635 (1998).
- [8] N. Stiesdal, J. Kumlin, K. Kleinbeck, P. Lunt, C. Braun, A. Paris-Mandoki, C. Tresp, H. P. Büchler, and S. Hofferberth, Observation of three-body correlations for photons coupled to a rydberg superatom, Phys. Rev. Lett. **121**, 103601 (2018).
- [9] Q.-Y. Liang, A. V. Venkatramani, S. H. Cantu, T. L. Nicholson, M. J. Gullans, A. V. Gorshkov, J. D. Thompson, C. Chin, M. D. Lukin, and V. Vuletić, Observation of three-photon bound states in a quantum nonlinear medium, Science **359**, 783 (2018).
- [10] D. P. Ornelas-Huerta, P. Bienias, A. N. Craddock, M. J. Gullans, A. J. Hachtel, M. Kalinowski, M. E. Lyon, A. V. Gorshkov, S. L. Rolston, and J. V. Porto, Tunable three-body loss in a nonlinear rydberg medium, Phys. Rev. Lett. **126**, 173401 (2021).
- [11] N. Tomm, S. Mahmoodian, N. O. Antoniadis, R. Schott, S. R. Valentin, A. D. Wieck, A. Ludwig, A. Javadi, and R. J. Warburton, Photon bound state dynamics from a single artificial atom, Nature Physics **19**, 857 (2023).
- [12] B. C. Das, A. Harkavi, A. Prakash, A. Nakav, L. Drori, and O. Firstenberg, Quantum nonlinear optics with counter-propagating photons, arXiv preprint arXiv:2506.01124 (2025).
- [13] G. Ferioli, S. Pancaldi, A. Glicenstein, D. Clément, A. Browaeys, and I. Ferrier-Barbut, Non-gaussian correlations in the steady state of driven-dissipative clouds of two-level atoms, Phys. Rev. Lett. **132**, 133601 (2024).
- [14] S. L. McCall and E. L. Hahn, Self-induced transparency, Phys. Rev. **183**, 457 (1969).
- [15] K. Hammerer, A. S. Sørensen, and E. S. Polzik, Quantum interface between light and atomic ensembles, Rev. Mod. Phys. **82**, 1041 (2010).
- [16] D. Goncalves, L. Bombieri, G. Ferioli, S. Pancaldi, I. Ferrier-Barbut, A. Browaeys, E. Shahmoon, and D. Chang, Driven-dissipative phase separation in free-space atomic ensembles, PRX Quantum **6**, 020303 (2025).
- [17] K. J. Kusmierek, M. Schemmer, S. Mahmoodian, and K. Hammerer, Emergence of unidirectionality and phase separation in optically dense emitter ensembles, arXiv preprint arXiv:2412.14930 (2024).
- [18] C. W. Gardiner, Driving a quantum system with the output field from another driven quantum system, Phys. Rev. Lett. **70**, 2269 (1993).
- [19] H. J. Carmichael, Quantum trajectory theory for cascaded open systems, Phys. Rev. Lett. **70**, 2273 (1993).
- [20] K. J. Kusmierek, S. Mahmoodian, M. Cordier, J. Hinney, A. Rauschenbeutel, M. Schemmer, P. Schneeweiss, J. Volz, and K. Hammerer, Higher-order mean-field theory of chiral waveguide qed, SciPost Phys. Core **6**, 041 (2023).
- [21] D. Plankensteiner, C. Hotter, and H. Ritsch, Quantum-cumulants. jl: A julia framework for generalized mean-field equations in open quantum systems, Quantum **6**, 617 (2022).
- [22] M. T. Manzoni, D. E. Chang, and J. S. Douglas, Simulating quantum light propagation through atomic ensembles using matrix product states, Nature communications **8**, 1743 (2017).
- [23] S. Mahmoodian, G. Calajó, D. E. Chang, K. Hammerer, and A. S. Sørensen, Dynamics of many-body photon bound states in chiral waveguide qed, Phys. Rev. X **10**, 031011 (2020).
- [24] V. I. Yudson, Dynamics of integrable quantum systems, Zh. Eksp. Teor. Fiz. **88**, 1757 (1985).
- [25] V. Rupasov and V. Yudson, Exact dicke superradiance theory: Bethe wavefunctions in the discrete atom model, Zh. Eksp. Teor. Fiz **86**, 819 (1984).
- [26] S. Weinberg, *The Quantum Theory of Fields: Volume I* (Cambridge University Press, 1995).
- [27] Y. Wang, N. Demazure, and S. Mahmoodian, Theory of three-photon transport through a weakly coupled atomic ensemble (2025), arXiv:2507.03428 [quant-ph].
- [28] V. I. Yudson and P. Reineker, Multiphoton scattering in a one-dimensional waveguide with resonant atoms, Phys. Rev. A **78**, 052713 (2008).
- [29] M.-A. Lemonde, N. Didier, and A. A. Clerk, Antibunching and unconventional photon blockade with gaussian squeezed states, Phys. Rev. A **90**, 063824 (2014).
- [30] K. Jachymski, P. Bienias, and H. P. Büchler, Three-body interaction of rydberg slow-light polaritons, Phys. Rev. Lett. **117**, 053601 (2016).
- [31] Y. Cardin and N. Quesada, Photon-number moments and cumulants of Gaussian states, Quantum **8**, 1521 (2024).
- [32] T. Shi, E. Demler, and J. Ignacio Cirac, Variational study of fermionic and bosonic systems with non-gaussian states: Theory and applications, Annals of Physics **390**, 245 (2018).
- [33] L. Hackl and E. Bianchi, Bosonic and fermionic Gaussian states from Kähler structures, SciPost Phys. Core **4**, 025 (2021).
- [34] Strictly, we require $\mathcal{O}(P_{\text{in}}/\Gamma_{\text{tot}}) = \mathcal{O}(\beta^2)$, but it is shown in the accompanying work [27] that this condition can be loosened to be $\mathcal{O}(P_{\text{in}}/\Gamma_{\text{tot}}) = \mathcal{O}(\beta)$.